SCIENTIFIC REPORTS

OPEN

SUBJECT AREAS:
MECHANICAL ENGINEERING
ATOMIC FORCE MICROSCOPY

Received
3 December 2013

Accepted
23 April 2014

Published
15 May 2014

Correspondence and requests for materials should be addressed to K.K. (kyokim@umich.edu) or P.R. (pramodr@umich.edu)

* These authors contributed equally to this work.

Characterization of nanoscale temperature fields during electromigration of nanowires

Wonho Jeong[1]*, Kyeongtae Kim[1]*, Youngsang Kim[1]*, Woochul Lee[1] & Pramod Reddy[1,2]

[1]Department of Mechanical Engineering, University of Michigan, Ann Arbor, MI 48109, USA, [2]Department of Materials Science and Engineering, University of Michigan, Ann Arbor, MI 48109, USA.

Quantitative studies of nanoscale heat dissipation (Joule heating) are essential for advancing nano-science and technology. Joule heating is widely expected to play a critical role in accelerating electromigration induced device failure. However, limitations in quantitatively probing temperature fields—with nanoscale resolution—have hindered elucidation of the role of Joule heating in electromigration. In this work, we use ultra-high vacuum scanning thermal microscopy to directly quantify thermal fields in nanowires during electromigration. Our results unambiguously illustrate that electromigration begins at temperatures significantly lower than the melting temperature of gold. Further, we show that during electromigration voids predominantly accumulate at the cathode resulting in both local hot spots and asymmetric temperature distributions. These results provide novel insights into the microscopic details of hot spot evolution during electromigration and are expected to guide the design of reliable nanoscale functional devices.

Understanding heat dissipation (Joule heating) and transport in nanoscale devices is critical for realizing novel nanoscale functional devices[1–3]. In fact, Joule heating is widely expected to play an important role in electromigration induced device failure: a process where atoms in a device are displaced due to momentum transfer between charge carriers and the lattice[4–14]. Electromigration in devices is always accompanied by Joule heating, which accelerates the electromigration process by affecting the mobility of atoms and is well known to limit the operating voltages and the reliability of functional devices[2,4,15]. Further, electromigration has also been utilized recently to create novel nanoscale electronic and memory devices[16–19]. To better understand the role of Joule heating on electromigration several research groups have indirectly estimated the local temperature changes during electromigration[8–10,12,20]. However, direct quantification of temperature fields during electromigration—with nanoscale resolution—has remained elusive although such knowledge is critical for both increasing the reliability of nanoscale devices and creating functional devices that take advantage of electromigration.

In this work, we leverage recent advances in ultra-high vacuum scanning thermal microscopy (UHV-SThM)[1,21,22] that enable quantitative nanoscale measurements of temperature fields. Using this technique, we probe temperature fields in prototypical bow-tie shaped gold (Au) devices (see Fig. 1a or 3a) that are widely used in molecular electronics for creating electromigrated break junction based molecular-scale devices[17,19,23,24] and in plasmonics for obtaining local enhancements in electric fields[25,26]. To elaborate, temperature measurements are performed (in the contact mode) using a custom fabricated scanning probe with an integrated thermocouple in two different schemes: (a) an unmodulated scheme (DC scheme) where the temperature field is not periodically modulated and (b) a modulated scheme (AC scheme) where the temperature field is periodically modulated at a frequency of 10 Hz. The DC scheme enables fast thermal measurements while achieving a somewhat lower temperature resolution (~2 K). Whereas, the AC scheme requires a relatively longer time (~85 minutes) to map the temperature fields but enables higher spatial (~10 nm) and temperature (~15 mK) resolutions, see Supplementary Information (SI) for more details. By employing these two schemes we performed experiments to obtain detailed information regarding both the temperature rise of local hot spots (where electromigration is initiated) and the spatial variations of temperature fields in nanoscale devices during electromigration.

Results

The schematic of the experimental setup is shown in Fig. 1a. The bow-tie shaped Au nanowires (~225 nm wide and ~450 nm long) were defined by e-beam lithography and evaporation (Ti/Au, 3/40 nm thick) on a Si wafer

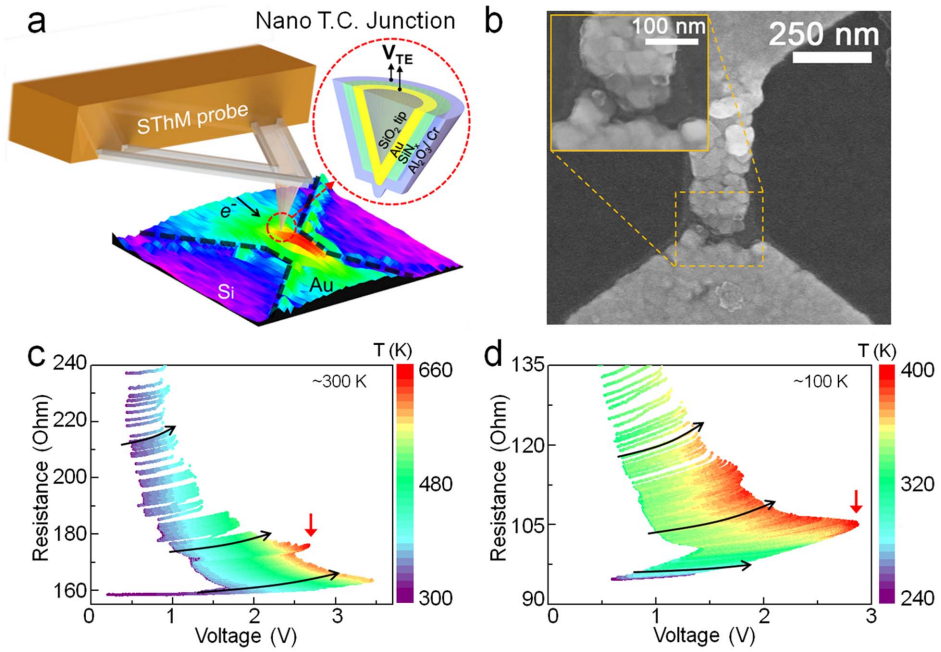

Figure 1 | Schematic of the measurement approach and data describing the local temperature rise during electromigration. (a) Schematic of the ultra-high vacuum scanning thermal microscopy used in this work. (b) A representative scanning electron microscope image of a nanogap junction after electromigration. (c) A two-dimensional color plot that captures the resistance change and the local temperature rise of the device when it is subjected to a cyclic voltage application (represented by black arrows) at room temperature. The point at which the maximum temperature attained is indicated by the red vertical arrow. (d) Similar data as in (c) obtained at a low temperature.

with a 500 nm thick thermally grown SiO_2 layer. Subsequently, source/drain electrodes were defined by photolithography and evaporation (Ti/Au, 3/70 nm thick) in order to ensure good electrical contact with the Au nanowires. The detailed fabrication process of SThM probes, with integrated gold-chromium thermocouples, can be found elsewhere[21]. In order to carry out thermal measurements during electromigration the bow-tie samples were placed in a UHV chamber, and all experiments were performed under UHV conditions ($<10^{-9}$ torr) at room temperature (~300 K) or at a low temperature (~100 K).

To perform electromigration we adopted a process originally developed by others[8,11,27]. Briefly, we applied a cyclic voltage to the Au nanowires of the bow-tie structure (Figs. 1c, d) while the electrical resistance was continuously monitored. The applied voltage was linearly ramped up in steps of 5 mV every 100 ms until the resistance increased by 1 ~ 5%. The threshold value was manually controlled depending on the monitored resistance of the nanowire samples. Upon detection of the desired increase in the resistance the voltage was rapidly ramped down. We note that the resistance of the device increased irreversibly as electromigration proceeded; this is in contrast to reversible changes in resistance due to temperature variations. This process was continued until the electromigration process was completed resulting in a nanoscale gap in the bow-tie devices as shown in Fig. 1b. The formation of a nanoscale gap is readily recognized by a rapid increase in the electrical resistance.

To measure the local temperature rise of the Au nanowires during the electromigration process, we first placed the SThM probe in mechanical contact with the bow-tie shaped devices at a contact force of 150 ± 25 nN. The contact location was chosen to be on the cathode side (*i.e.* the electrode from which electrons enter the nanowire) at a point that is ~100 nm from where the cathode meets the nanowire as illustrated in Fig. 1a. This location is well suited because: 1) it is sufficiently close to the nanowire to record temperatures that are representative of the local temperature rise of the nanowire, 2) this is the region where the temperature rise is the largest after electromigration (as explained in detail later), and 3) the measured temperature signal is not affected by the electromigration induced topographical changes of the devices. The temperature rise of the nanowires was recorded *via* the thermocouple integrated into the probe while a cyclical voltage was applied to the bow-tie devices to initiate electromigration. The voltage output of the integrated thermocouple (ΔV) is related to the local temperature rise (ΔT) by $\Delta T \times \beta = |\Delta V|/S_T$, where $S_T = 16.3 \pm 0.1$ μV/K is the Seebeck coefficient of the thermocouple and $\beta = 0.083 \pm 0.006$ K/K is the sensitivity of the probe (see SI)[21].

Fig. 1c shows a two-dimensional color plot of the measured local temperature rise and evolution of the electrical resistance as the applied voltage is cycled at room temperature. Data obtained in a similar experiment performed at a lower temperature (~100 K) are shown in Fig. 1d. Since the thermal time constant of the SThM probe is sufficiently small (<100 ms)[21], it tracks the variations in the local temperatures with high fidelity. It can be seen from Figs. 1c, d that the maximum temperature attained during electromigration in both the high and low temperature measurements occurs when the resistance changes by ~10%. Specifically, the maximum local temperature is ~660 K for the experiment performed at room temperature and ~400 K for the experiment performed at a low temperature (~100 K), which were measured at the location aforementioned. From the data shown in Figs. 1c, d, it is clear that the overall trends of temperature rise during electromigration are relatively independent of the ambient temperature. However, the maximum temperature rise observed during electromigration is significantly smaller in low temperature measurements—a fact that can be leveraged in creating molecule-based devices where a large increase in the local absolute temperature is detrimental to the stability of molecules[19,20].

An important question to address in this context is: What is the local temperature of hot spots at which electromigration is actually initiated? In order to answer this question it is instructive to present the data shown in Figs. 1c, d in a different form that enables visualization of the relationship between the resistance change and the temperature rise. Therefore, in Figs. 2a–d we present the measured temperature rise as a function of the resistance of the device during

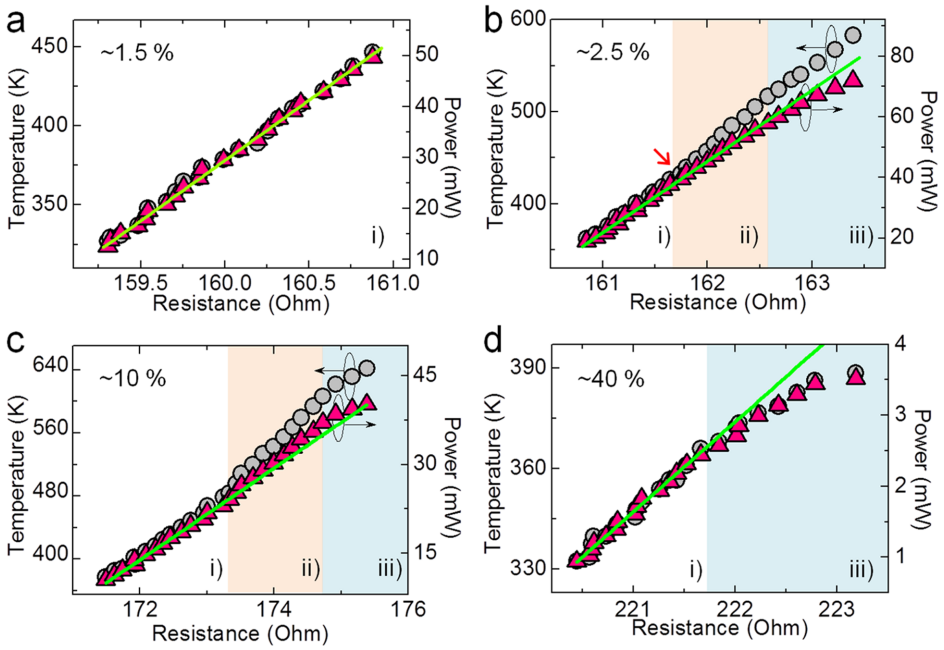

Figure 2 | Local temperature rise profiles during electromigration. (a) – (d) The traces relating both the temperature and power dissipation to the device resistance during electromigration. The traces were obtained at various stages of electromigration where the device resistance increased by 1.5%, 2.5%, 10% and 40%, respectively. The green line is obtained by fitting the temperature vs. resistance data at small power dissipations and is provided to facilitate visualization of deviations from linearity.

electromigration. In Fig. 2a, it can be seen that before electromigration is initiated the temperature increases approximately linearly with the resistance. In contrast, for the devices where the resistance had irreversibly changed by 2.5% or 10% (Figs. 2b, c), the relationship between temperature and resistance as well as that between power dissipation and resistance were found to be non-linear. The onset of the nonlinearity in the relationship between temperature and resistance is highlighted by a red arrow in Fig. 2b and indicates the point at which electromigration is initiated when the local temperature of the nanowires reached ~430 K. Similar analysis of the data obtained in low temperature measurements indicates that electromigration is initiated at ~315 K. In addition, the temperature and power dissipation traces which are scaled to overlap at lower powers do not continue to overlap with each other in the shaded regions in Fig. 2b, c. This is due to the fact that upon additional electromigration Joule heating is more localized to regions where voids accumulate thus changing the relationship between the temperature measured by the probe and the total power dissipation. Further, from FEM simulations we estimated that the temperature rise (before electromigration) at the middle of the nanowire is ~20% larger than what we measured at the location shown in Fig. 1a (see SI). This implies that the local temperature in the hot spots when electromigration starts is ~520 K in room temperature measurements and ~380 K in low temperature measurements. These values are larger than those reported in previous studies[10,20,28]. This deviation can be attributed to the indirect way in which previous temperature measurements were performed that resulted in a spatial average of the device temperature, which is lower than the local temperature in the hot spots. Our results clearly show that electromigration of Au nanowires is indeed initiated at temperatures much lower than the melting temperature of Au (~1337 K)[29], which indicates that the electric field contributes dominantly to electromigration.

In order to obtain further insights, we performed additional experiments where we first terminated the electromigration process at certain representative states (the resistance of the devices had increased by 2.5%, 10% and 40%, respectively). Subsequently, we mapped the topography and temperature fields of the devices under

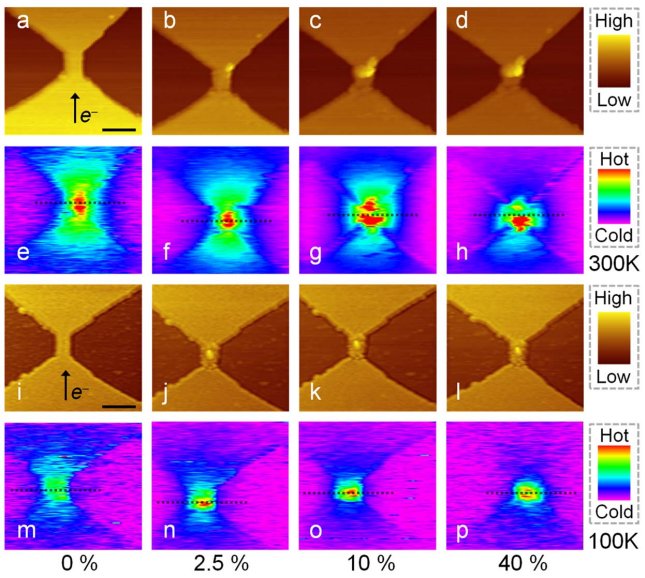

Figure 3 | Topographic and thermal images during electromigration. (a)–(d) and (i)–(l) show the topography of nanowire devices at various stages of electromigration performed at room temperature (~300 K) and a low temperature (~100 K), respectively. (e)–(h) and (m)–(p) are the thermal images obtained under a small sinusoidal bias at ambient temperatures of ~300 K and ~100 K, respectively. The maximum temperatures of (e)–(h) and (m)–(p) are 311.4 K, 328.2 K, 385.8 K, 346.8 K, 108.2 K, 111.9 K, 122.2 K and 115.9 K, respectively. The temperature fields of Au nanowires were observed to change from symmetrical ((e)–(g) and (m)–(o)) to asymmetrical ((h) and (p)), about the dotted center line, as electromigration proceeded. The direction of electron flow (from cathode to anode) is indicated by the black arrow. The scale bar corresponds to 500 nm.

a small sinusoidal bias voltage with an amplitude <0.3 V and a frequency of 5 Hz. The applied voltage bias was sufficiently small that no further electromigration occurs during thermal characterization. The topography was obtained in contact mode at a contact force of 150 ± 25 nN while the temperature fields were mapped by locking in to the second harmonic component (10 Hz) of the voltage output from the integrated thermocouple (see ref 21 for more details).

The obtained topography for Au nanowires when the resistance of the device had changed by 0%, 2.5%, 10% and 40% are shown in Figs. 3a–d, respectively. The measured topography unambiguously shows the formation of hillocks and depressions, which mostly emerged at an early stage of the electromigration process where the resistance increase was <10%. The corresponding temperature fields are shown in Figs. 3e–h, which highlight an important feature: an increase in the asymmetry of the temperature fields upon electromigration. Specifically, before electromigration the temperature fields are symmetrical about the center line (the dotted line) with the maxima of the temperature fields being located in the middle of the nanowire. However, as electromigration progresses and results in a 40% resistance change, the temperature fields become increasingly asymmetric with the temperature rise being larger at the intersection of the nanowire and the cathode. The color codes used in Figs. 3e–h and 3m–p represent normalized temperature rises with red being hotter than blue. The increase in the asymmetry of the temperature fields can be qualitatively understood by hypothesizing that voids/vacancies are created and accumulated primarily in the cathode of the device (see SI). This hypothesis is consistent with previous studies that have observed the accumulation of voids in nanoscale devices[9,10,13,14,30].

Further, thermal imaging measurements performed at a low temperature (~100 K) show similar trends (Figs. 3m–p). However, in this case the asymmetry in the temperature fields is less prominent than the measurements performed at room temperature. These results can be partly understood by noting that the mobility of Au atoms is lower at 100 K than room temperature, which requires a larger current density for initiating electromigration[10] (as experimentally observed, ~1.9×10^{12} A/m^2 for low temperature measurements versus ~1.3×10^{12} A/m^2 for room temperature measurements). We believe that this large current density creates voids both in the cathode and in the nanowire leading to a less asymmetrical temperature field. In spite of this reduced asymmetry in the temperature fields, we note that the location of nanogap formation still showed the same bias-polarity dependence *i.e.* the voids accumulated primarily in the cathode. The fact that there are similar trends in the low and high temperature measurements is consistent with the view point that electromigration is primarily driven by the electric field and the ambient temperature plays a less significant role.

Finally, we note that we have limited our topography and thermal imaging studies to the devices whose resistances have changed by 40% or less because the voltage required for obtaining appreciable temperature changes increases with increasing resistance. In general, large voltages tend to induce further electromigration preventing thermal imaging of devices before the resistance increases further.

Discussion

The above results raise an important question: What is the source of the observed asymmetry in the temperature fields after electromigration? Is it due to the formation of a crack/notch in the electrode or caused by a local change in the electrical resistivity resulting from the accumulation of voids, which enhance electron scattering and increase heat dissipation? In order to answer this question, we performed finite element modeling (FEM) simulations using COMSOL (Joule heating module). In these simulations, we first considered the case where a notch is developed in the nanowire without a change in the local electrical resistivity (see Methods for details). The computed temperature field when a current density of 1.3×10^{11} A/m^2, which is comparable to that used in our scanning measurements, is applied

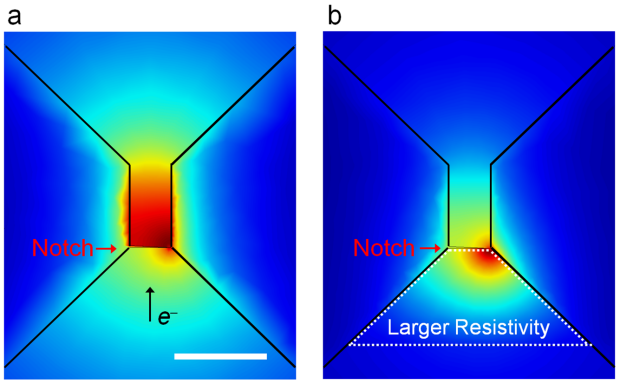

Figure 4 | Results of finite element modeling performed to simulate the effect of structural change and increased electrical resistivity. (a) The temperature field obtained from a finite element modeling simulation of a notched nanowire shows no appreciable asymmetry. (b) Similar modeling performed for a nanowire with both a notch and a local increase in the electrical resistivity of the highlighted region (marked by a dotted line) of the cathode by ten times (to 2.2×10^{-7} Ω·m). In this case an asymmetrical temperature field is observed. The scale bar corresponds to 500 nm.

across such a notched nanowire is shown in Fig. 4a. It can be clearly seen that the temperature field is largely symmetric highlighting that structural effects alone—*i.e.* notch formation as the breakdown proceeds—cannot explain the asymmetrical temperature fields observed in the experiments. For comparison, we performed a second FEM simulation (Fig. 4b) where in addition to the notch, the local electrical resistivity of the cathode was increased by a factor of ten to 2.2×10^{-7} Ω·m—to mimic the effect of accumulation of voids—in the region of the cathode highlighted by the dotted line in Fig. 4b. It can be seen that the modeled temperature field is asymmetric in correspondence with experimental observations providing strong support for our hypothesis of voids accumulation in the cathode during electromigration. This hypothesis can also be understood using a simple model that is discussed in the SI.

Additional insights into the breakdown mechanism of Au nanowires during electromigration can be obtained by a more detailed analysis of the data in Figs. 2a–d. Before the initiation of electromigration (Fig. 2a), it is clear that the resistance and the temperature change are linearly related. This should be expected because for a metallic wire the relationship between the temperature rise (ΔT) and the resistance (R) is given by,

$$R = R_0(1 + \alpha \Delta T) \quad (1)$$

where R_0 is the wire resistance when ΔT is zero, and α is the temperature coefficient of resistance (TCR) of the metallic wire. This implies that,

$$\frac{dT}{dR} = \frac{1}{\alpha R_0} \quad (2)$$

therefore, if αR_0 changes, the slope (dT/dR) becomes non-linear. As mentioned above, in Fig. 2a the temperature and power dissipation traces overlap with each other and show a linear dependence on the nanowire resistance because the resistance change is dominated by Joule heating. The range where this linear relation appears is marked as region i) in Figs. 2a–d.

In addition, from the data shown in Figs. 2b, c, it is clear that immediately after the initiation of electromigration both the resistance and the slope (dT/dR) increase implying that the TCR decreases (indicated as region ii)). This observed decrease in TCR can be attributed to our hypothesis of voids creation that results in a reduced electron mean free path, which is known to suppress TCR[31,32]. It can be also seen in Figs. 2b, c that at larger temperature rises, which

correspond to higher voltage biases (marked as region iii)), the slope of the temperature (dT/dR) and power dissipation (dP/dR) curves decrease simultaneously. This can be understood by noting that an increased electrical resistance due to voids accumulation reduces the overall Joule heating in the device. This behavior was also observed in Fig. 2d for the device where the resistance had changed by 40%.

In conclusion, by employing UHV-SThM we successfully studied temperature fields in Au nanowires during electromigration at both room temperature (~300 K) and a low temperature (~100 K). From these measurements, we were able to obtain information regarding both the local temperature rise and spatial inhomogeneity of electrical resistivity in the nanowires during electromigration. Specifically, the later information was obtained by thermally imaging the nanowires under a small sinusoidal bias to elucidate asymmetries in temperature fields that are directly related to the local electrical resistivity. We also found that the maximum absolute temperature at the onset of electromigration can be substantially suppressed by lowering the ambient temperature. Further, our results provide strong evidence for accumulation of voids in the cathode of the devices during electromigration, which results in the preferential nanogap formation on the cathode. The experimental approach reported here enables deeper insights into the role of Joule heating (heat dissipation) in the failure of nanoscale devices. This approach can be applied to investigate a variety of interesting heat related phenomena relevant to many areas of nano-science and technology.

Methods

Finite element modeling (FEM) simulations. To compute temperature fields of the nanowire devices, we used commercial FEM software COMSOL (Joule heating module). An electrical current was simulated through the Au nanowire from the source electrode to the drain electrode, while all other surfaces were electrically insulated. In addition, the temperature of the bottom surface (of the 500 μm thick Si wafer on which the nanowire is located) was modeled to be at 300 K, while all other surfaces were modeled to be thermally insulating. The thermal conductivity and electrical resistivity of materials were chosen to be 320 W/m·K and 2.2×10^{-8} Ω·m respectively for bulk Au and 160 W/m·K and 4.4×10^{-8} Ω·m respectively for thin film Au in the bow-tie region[33]. Further, the thermal conductivity of Si and SiO_2 were assigned to be 150 W/m·K and 1.4 W/m·K, respectively[34].

1. Lee, W. *et al.* Heat dissipation in atomic-scale junctions. *Nature* **498**, 209 (2013).
2. Costa, P. M. F. J., Gautam, U. K., Bando, Y. & Golberg, D. Direct imaging of Joule heating dynamics and temperature profiling inside a carbon nanotube interconnect. *Nat. Commun.* **2**, 421 (2011).
3. Seol, J. H. *et al.* Two-Dimensional Phonon Transport in Supported Graphene. *Science* **328**, 213–216 (2010).
4. Tao, C. G., Cullen, W. G. & Williams, E. D. Visualizing the Electron Scattering Force in Nanostructures. *Science* **328**, 736–740 (2010).
5. Nam, S. W. *et al.* Electrical Wind Force-Driven and Dislocation-Templated Amorphization in Phase-Change Nanowires. *Science* **336**, 1561–1566 (2012).
6. Park, H., Lim, A. K. L., Alivisatos, A. P., Park, J. & McEuen, P. L. Fabrication of metallic electrodes with nanometer separation by electromigration. *Appl. Phys. Lett.* **75**, 301–303 (1999).
7. Strachan, D. R. *et al.* Real-time TEM imaging of the formation of crystalline nanoscale gaps. *Phys. Rev. Lett.* **100**, 056805 (2008).
8. Esen, G. & Fuhrer, M. S. Temperature control of electromigration to form gold nanogap junctions. *Appl. Phys. Lett.* **87**, 263101 (2005).
9. Durkan, C., Schneider, M. A. & Welland, M. E. Analysis of failure mechanisms in electrically stressed Au nanowires. *J. Appl. Phys.* **86**, 1280–1286 (1999).
10. Trouwborst, M. L., van der Molen, S. J. & van Wees, B. J. The role of Joule heating in the formation of nanogaps by electromigration. *J. Appl. Phys.* **99**, 114316 (2006).
11. Hoffmann, R., Weissenberger, D., Hawecker, J. & Stoffler, D. Conductance of gold nanojunctions thinned by electromigration. *Appl. Phys. Lett.* **93**, 043118 (2008).
12. Ward, D. R., Halas, N. J. & Natelson, D. Localized heating in nanoscale Pt constrictions measured using blackbody radiation emission. *Appl. Phys. Lett.* **93**, 213108 (2008).
13. Heersche, H. B., Lientschnig, G., O'Neill, K. & van der Zant, H. S. J. In situ imaging of electromigration-induced nanogap formation by transmission electron microscopy. *Appl. Phys. Lett.* **91**, 072107 (2007).
14. Stahlmecke, B. *et al.* Electromigration in self-organized single-crystalline silver nanowires. *Appl. Phys. Lett.* **88**, 053112 (2006).
15. Tu, K. N. Recent advances on electromigration in very-large-scale-integration of interconnects. *J. Appl. Phys.* **94**, 5451–5473 (2003).
16. Xiong, F., Liao, A. D., Estrada, D. & Pop, E. Low-Power Switching of Phase-Change Materials with Carbon Nanotube Electrodes. *Science* **332**, 568–570 (2011).
17. Song, H. *et al.* Observation of molecular orbital gating. *Nature* **462**, 1039–1043 (2009).
18. Osorio, E. A. *et al.* Electronic excitations of a single molecule contacted in a three-terminal configuration. *Nano Lett.* **7**, 3336–3342 (2007).
19. Cuevas, J. C. & Scheer, E. Molecular electronics: an introduction to theory and experiment. (World Scientific, Singapore; 2010).
20. Taychatanapat, T., Bolotin, K. I., Kuemmeth, F. & Ralph, D. C. Imaging electromigration during the formation of break junctions. *Nano Lett.* **7**, 652–656 (2007).
21. Kim, K., Jeong, W. H., Lee, W. C. & Reddy, P. Ultra-High Vacuum Scanning Thermal Microscopy for Nanometer Resolution Quantitative Thermometry. *ACS Nano* **6**, 4248–4257 (2012).
22. Kim, K., Chung, J., Hwang, G., Kwon, O. & Lee, J. S. Quantitative Measurement with Scanning Thermal Microscope by Preventing the Distortion Due to the Heat Transfer through the Air. *ACS Nano* **5**, 8700–8709 (2011).
23. Bolotin, K. I., Kuemmeth, F., Pasupathy, A. N. & Ralph, D. C. From ballistic transport to tunneling in electromigrated ferromagnetic breakjunctions. *Nano Lett.* **6**, 123–127 (2006).
24. Liang, W. J., Shores, M. P., Bockrath, M., Long, J. R. & Park, H. Kondo resonance in a single-molecule transistor. *Nature* **417**, 725–729 (2002).
25. Ward, D. R., Corley, D. A., Tour, J. M. & Natelson, D. Vibrational and electronic heating in nanoscale junctions. *Nature Nanotech.* **6**, 33 (2011).
26. Coppens, Z. J., Li, W., Walker, D. G. & Valentine, J. G. Probing and controlling photothermal heat generation in plasmonic nanostructures. *Nano Lett.* **13**, 1023–1028 (2013).
27. Strachan, D. R. *et al.* Controlled fabrication of nanogaps in ambient environment for molecular electronics. *Appl. Phys. Lett.* **86**, 043109 (2005).
28. Durkan, C. & Welland, M. E. Analysis of failure mechanisms in electrically stressed gold nanowires. *Ultramicroscopy* **82**, 125–133 (2000).
29. Ashcroft, N. W. & Mermin, N. D. Solid State Physics. (Cengage Learning, New York; 1976).
30. Stoffler, D., Fostner, S., Grutter, P. & Hoffmann-Vogel, R. Scanning probe microscopy imaging of metallic nanocontacts. *Phys. Rev. B* **85**, 033404 (2012).
31. Zhang, Q. G. *et al.* Influence of grain boundary scattering on the electrical properties of platinum nanofilms. *Appl. Phys. Lett.* **89**, 114102 (2006).
32. Zhang, X., Song, X. H., Zhang, X. G. & Zhang, D. L. Grain boundary resistivities of polycrystalline Au films. *Eur. Phys. Lett.* **96**, 17010 (2011).
33. Chen, G. & Hui, P. Thermal conductivities of evaporated gold films on silicon and glass. *Appl. Phys. Lett.* **74**, 2942 (1999).
34. Incropera, F. P., DeWitt, D. P., Bergman, T. L. & Lavine, A. S. Fundamentals of Heat and Mass Transfer, Edn. 6th. (John Wiley & Sons Incorporated, 2006).

Acknowledgments

P.R. acknowledges support from US Department of Energy, Office of Basic Energy Sciences, Division of Materials Sciences and Engineering under award no. DE-SC0004871 (nanofabrication of scanning probes), DARPA under award no. N66001-12-1-4223 (fabrication of nanoscale devices) and AFOSR under award no. FA9550-10-1-0528 (development of an electromigration platform). Y.K. thanks R. Hoffmann for providing an initial version of electromigration program. All authors acknowledge the Lurie Nanofabrication Facility (LNF) for facilitating the fabrication of SThM probes and nanowire samples.

Author contributions

P.R. and K.K. planed and supervised the project. W.J., K.K., Y.K. and W.L. performed the experiments and interpreted the data. W.J. and Y.K. fabricated the nanowire samples. W.J. performed FEM simulations. W.J., Y.K., K.K. and P.R. wrote the manuscript with comments and inputs from all authors.

Additional information

Competing financial interests: The authors declare no competing financial interests.

How to cite this article: Jeong, W., Kim, K., Kim, Y., Lee, W. & Reddy, P. Characterization of nanoscale temperature fields during electromigration of nanowires. *Sci. Rep.* **4**, 4975; DOI:10.1038/srep04975 (2014).